Optical sensing based on phase interrogation with a Young's interference hologram using a digital micromirror device

Théo Girerd, Fabien Mandorlo, Cécile Jamois, T. Benyatou, Lydie Ferrier, Lotfi Berguiga

Research Article Vol. 32, No. 3 / 29 Jan 2024 / Optics Express 3647
Optics EXPRESS

Optical sensing based on phase interrogation with a Young's interference hologram using a digital micromirror device

THÉO GIRERD,[1] FABIEN MANDORLO,[1] CÉCILE JAMOIS,[2] TAHA BENYATTOU,[2] LYDIE FERRIER,[1] AND LOTFI BERGUIGA[2,*]

[1] *Univ. Lyon, INSA Lyon, ECL, CNRS, UCBL, CPE Lyon, INL, UMR5270, 69621 Villeurbanne, France*
[2] *Univ. Lyon, CNRS, INSA Lyon, Ecole Centrale de Lyon, Université Claude Bernard Lyon 1, CPE Lyon, INL, UMR5270, 69621 Villeurbanne, France*
[*] *lotfi.berguiga@insa-lyon.fr*

Abstract: We propose a new holographic interferometric technique of phase interrogation for nanophotonic sensors, allowing to reach low phase noise and fluctuation by using a digital micromirror device spatial light modulator. With the spatial light modulator, both beam shaping and phase shifting interferometry can be simultaneously managed, hence enabling the interrogation of nanophotonic devices with a common-path heterodyne Young's interference experiment. The efficiency of the technique is illustrated in the particular case of temperature sensing using Tamm plasmon photonic crystals. The hologram sensor allows to probe resonant structures with deep attenuation at resonance, such as resonant structures at critical coupling or with phase singularities.

1. Introduction

Providing optical sensors with improved sensitivity and high-throughput is still a strategic challenge in medical diagnostics for the early monitoring of cancers and other diseases [1]], as well in environmental applications for the detection of gazes and volatile organic compounds (VOC) in very small concentrations [2]. Refractive index sensing is an efficient method for the detection species near an interface, which can yield very high sensitivity when coupled with a resonant effect. Many resonant refractive-index transducers have been developed, historically starting with surface plasmon resonance (SPR) [3] and waveguide sensors [4], and more recently metallic nanoparticles [5] and nanophotonic systems such as photonic crystals (PCs) [6,7]. In order to improve the limit of detection (LOD) of these systems, i.e., the smallest amount of species or molecules that can be measured, both the optical response of the transducer and the measurement method have to be considered. Improving the optical transducer is still an active area of research, and common figures of merit (FOM) have been introduced to compare the sensitivities of the different optical sensors [7]. Regarding the measurement method, it is assumed that phase measurement achieves a better limit of detection by several orders of magnitude compared to intensity interrogation [8–10]. To access the phase of the optical response, interferometric or polarimetric techniques must be used. Interferometric measurements have been proposed for VOC detection even without resonant transducers, and a review can be found in [11]. In the case of resonant sensors, interferometric methods have been used with SPR by many groups since 1999 [8–10,12], enabling to reach LODs as low as 10^{-8} refractive index unit (RIU) [9,13]. Interferometric methods have also been used with waveguide sensors, yielding LODs within the 10^{-8} RIU range when the light propagates the probed area over several millimeters [4,14]. Over the past decade, phase interrogation methods have also been applied for nanophotonics, e.g., plasmonic metasurfaces with ellipsometry [15] and interferometry interrogation [16], photonics crystals supporting guided mode resonances in interferometric

#507643 https://doi.org/10.1364/OE.507643
Journal © 2024 Received 6 Oct 2023; revised 16 Nov 2023; accepted 16 Nov 2023; published 19 Jan 2024

Optics EXPRESS

systems [17–19] or Tamm-plasmon structures with polarimetric methods (ellipsometry in this case) [20]. Although the interferometric techniques lead to better LODs than polarimetric methods that use commercial ellipsometers, the techniques based on interferometers are not protected from fluctuations; hence phase measurements can be unstable. Barth et al. [19] overcome this issue by proposing a differential interferometric measurement. In the present work, we propose a new interferometric measurement method that also tackles the fluctuation issues, allowing to reach LODs at the state of the art of phase measurement techniques with a high stability. The originality of the technique lies in the fact that it is both i) a common path interferometer, and ii) a phase shift interferometer (or pseudo-heterodyne interferometer). It is based on a Young's interferometer where the incident beam is shaped into two beams. All these simultaneous optical functions are enabled by the use of a spatial light modulator (SLM). SLMs are a powerful tool to manipulate the wavefront of light with high definition: the phase and/or amplitude of the reflected light can be reconfigured, allowing to obtain a large range of optical functions like display, beam steering, wavefront correction [21], wavefront shaping, spatial or temporal beam shaping, point spread function engineering in microscopy, hologram generation, or spatial polarization control (see reference [22] and references therein). Mainly, two types of technology coexist for SLMs: liquid crystal on silicon SLM (LCOS-SLM) and digital micromirror device SLM (DMD-SLM). Although LCOS-SLMs have already been used as phase shifting interferometers, e.g. for wavefront analysis of propagating light trough a multimode optical fiber [23], SLMs are still little used in sensor application: only in SPR for steering the angle of illumination [24] or in guided-mode resonance sensing for phase shifting interferometry [25]. To the best of our knowledge, this is the first time that a SLM is used to process several functions at the same time (phase modulation and beam shaping) for sensor application. In the proposed phase measurement method, a DMD-SLM is used to generate a sequence of holograms that is perturbed in presence of the sensor. The hologram sequence is then analyzed to extract the time-dependent amplitude and phase information. This method can be applied to any type of photonic structures, resonant or not. Our measurement is very well suited for photonic sensor fabricated by microelectronic process where sensor size is of few up to hundred micrometers. Thanks to the beam shaping by the SLM, a large scale of structures can be excited, with footprints ranging from several hundred μm down to a few micrometers. This method can be applied for various optical responses (even resonant structures that present a drastic intensity decrease at the resonance). As a proof of principle, we apply this new measurement method to a photonic crystal sensor based on a Tamm plasmon structure to show that high performance can be obtained.

The paper is organized as follow: in a first part, we present the underlying theory for the Young's interference and the principle of the hologram generation to produce the heterodyne Young's interferometer. In a second part, we present our two experimental configurations and we show the efficiency of the technique regarding phase noise and fluctuations. In a third part, experimental validation is provided via phase measurement on a Tamm plasmon photonic crystal used as a temperature sensor.

2. Hologram sensor theory

Our interferometric method for phase measurement relies on two distinct functions that are both ensured by the SLM:

- Holographic generation of two beams for the Young's interference,
- Phase modulation of one of the two beams, in order to recover the absolute phase via phase shifting interferometry.

These two functions will be presented in more details in the following. It should be noted that in the proposed technique, the phase measurement of the sensor response is not usual, since

Optics EXPRESS

wavefront and beam shaping are involved. If we reformulate the principle of the optical sensor, the measurement starts with a hologram input $I_{in}(x, y, t)$ and ends with a perturbed hologram output $I_{out}(x, y, t)$ when passing through the sensor and the analyte medium. By analyzing this perturbation of the holograms we can extract the amplitude and the phase of the electric field interacting with the transducer.

2.1. Young's interferences on a photonic sensor

For clarity purposes, the principle of the interferometric measurement presented in the following is only detailed in the case of a transmission configuration. However, a similar principle could be used in reflection. As shown in Figure YoungInterferencePrinciplea) the Young's interference is obtained from two Gaussian beams that are normally incident on a sample containing the photonic sensor and the analyte. A first Gaussian beam ('test' beam) illuminates the sensor, while a second Gaussian beam ('reference' beam) illuminates the substrate in the vicinity of the first beam but outside the sensor. The two beams interfere after passing through a lens. In the sample plane, the two spots can be considered as two Young's holes, hence resulting in a Young's interference in the focal plane of the lens. In this focal plane, the interference has an intensity profile (Figure 1(b)) that can be described by the following equation:

$$I_{out}(x, y) = I_0 \Upsilon(x, y) \left[A_{ref}^2 + (sA_{test})^2 + 2sA_{ref}A_{test} \cos\left(2\pi \frac{x}{\Lambda} + \phi_{ref} - \phi_{test}\right)\right] \tag{1a}$$

$$\text{with:} \quad I_0 = cste, \ \Upsilon(x, y) = e^{-\frac{2(x^2+y^2)}{\omega_h^2}}, \ \text{and } \Lambda = \frac{\lambda f}{D}, \ \text{and } \omega_h = \frac{\lambda f}{\pi a} \tag{1b}$$

with D the center-to-center distance between the two beams, a the waist of the two Gaussian beams, A_{test} and A_{ref} the amplitude of the two Gaussian beams, s the module of the transmission coefficient of the sensor, and ϕ_{test} and ϕ_{ref} the phase of the two beams after transmission through the sample. The envelop of the interference pattern is a Gaussian curve $\Upsilon(x, y)$ with width at $1/e^2$ equal to $2\omega_h$. Λ is the spacing between fringes. The width of the envelop interference pattern $2\omega_h$ is inversely proportional to the width of the initial Gaussian beam $2a$, whereas the fringe distance Λ is inversely proportional to the distance D between the two beams, as shown in Eq. (1b). Consequently, the number of fringes inside the envelop is directly related to the ratio D/a. The visibility (i.e the contrast) of the fringes is governed by s since the arm are initially balanced i.e. $A_{test} = A_{ref}$. If $s = 1$ the fringes go down to zero: the contrast is maximal and when s diminish to zero, the contrast fades until their disappearance. The position of the fringes inside the envelop are related to the phase difference $\phi_{test} - \phi_{ref}$ and when it changes the fringes slides laterally inside the envelop. Any change in the phase of the electric field from the photonic sensor induced by minute local refractive index changes at the sensor interface will lead to a sliding of the fringes inside the envelop. In order to quantify this phase change, two improvements are added to the Young's interference principle. The first improvement is a time modulation of the phase of one of the two beams (here the reference beam) at frequency f_{mod}:

$$\phi_{ref}(t) \equiv 2\pi f_{mod} \cdot t \pmod{2\pi} \tag{2}$$

It leads to a periodic sliding in the direction x of the Young's interference pattern as follows:

$$I_{out}(x, y, t) = I_0 \Upsilon(x, y) \left[A_{ref}^2 + (sA_{test})^2 + 2sA_{ref}A_{test} \cos\left(2\pi \frac{x}{\Lambda} + 2\pi f_{mod} \cdot t - \phi_{test}\right)\right] \tag{3}$$

The second improvement is to place a pinhole at the center of the Young's interference pattern, and to collect the light going through the pinhole by a photodetector. The variation of the signal

Optics EXPRESS

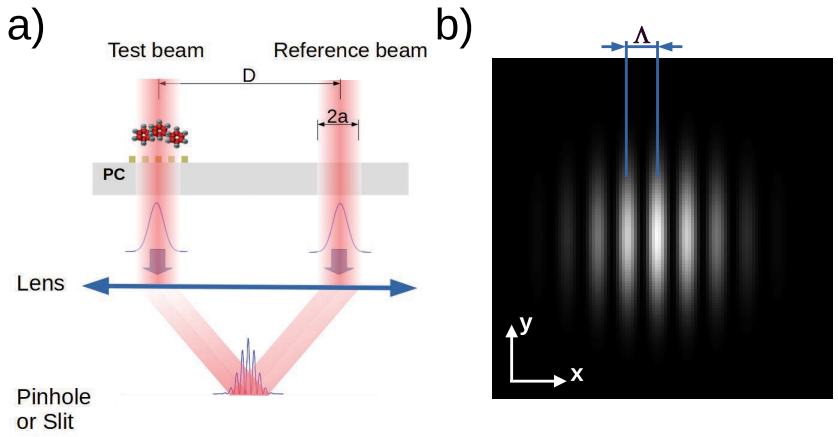

Fig. 1. Young's interference on a photonic sensor (here a photonic crystal labelled 'PC'): a) schematic view of the principle, b) example of intensity pattern at the focal plane of the lens

at the output of the photodiode will be proportional to:

$$I_c(t) \approx I_{out}(0,0,t) = I_0 \left[A_{ref}^2 + (sA_{test})^2 + 2sA_{ref}A_{test}\cos\left(2\pi f_{mod}\cdot t - \phi_{test}\right)\right] \quad (4)$$

To summarize, the interferometric signal I_c is modulated in time as a sinusoidal curve at the frequency f_{mod}. By demodulating this signal, we can extract the temporal changes of the phase and amplitude in the transmission of the photonic sensor (s and ϕ_{test}).

2.2. Hologram generation for Young's interferometry

The simplest way to generate two beams, with the first one adapted to the size of the photonic sensor and the second one used as a reference, is to perform direct beam shaping of an incident beam with the help of a SLM. However, this straightforward method is not efficient since the dimension of the targeted spot beams (few to tens of micrometers) are small compared to the SLM resolution and will also lead to a poor reflectivity efficiency on the SLM. Actually, very few pixels of the SLM would contribute to the shaping of the incoming beam. To overcome this issue, our strategy consists in shaping the Fourier transform of the two targeted beams, which corresponds to a Young's interference pattern ($I_{in}(x,y)$). This way, the pattern illuminates the whole area of the SLM instead of a few pixels. The hologram $I_{in}(x,y,t)$ introduced at the input of the hologram sensor system follows this equation:

$$I_{in}(x,y,t) = I_0.\Upsilon(x,y)\left[A_{ref}^2 + (A_{test})^2 + 2A_{ref}A_{test}\cos\left(2\pi\frac{x}{\Lambda} + 2\pi f_{mod}\cdot t\right)\right] \quad (5)$$

In the following discussion, we consider that the power of the two Gaussian beams are well-balanced, i.e $A_{ref} = A_{test}$. The Young's interference pattern used as an input looks like the pattern of figure 1(b). In this work, we choose a digital micro-mirror device (DMD) SLM, as it offers faster responses compared to LCOS-SLM. A DMD is a 2D matrix of micro-mirrors that switch between two orientations on a pivot and deflect light in two directions at ±12°, corresponding to the 'on' and 'off' positions. The pattern that is encoded into the SLM is a binary pattern. To provide the original Young's interference pattern $I_{in}(x,y)$ (which is an analogic signal) from a binary pattern, an encoding step is required. In general, the Lee method [26] or the super pixel method [27] are used to produce the wanted analogical complex electric field (the hologram) from a binary pattern. Here we choose the Lee method, which is a nonlinear filter

Optics EXPRESS

that computes a diffracting binary pattern as an output from the targeted hologram input $I_{in}(x, y)$. When the SLM encoded with the binary pattern is illuminated, many orders of diffraction are excited and the targeted field $I_{in}(x, y)$ can be recovered in the first order. Figure 2 describes the general principle that has been implemented to generate the Young's interference hologram $I_{in}(x, y)$ and the two Gaussian beams that illuminate the photonic sample. In a first step we numerically construct the two Gaussian beams with their expected dimensions a and D, as well as their expected phases (Figure 2(a)). Then we generate the Young's interferometric pattern $I_{in}(x, y)$ by a Fourier transformation (figure 2(b)). The binary hologram used to encode the SLM with on and off mirror positions is numerically generated by Lee's algorithm with $I_{in}(x, y)$ as an input pattern. The resulting binary pattern is shown Figure 2(c). After encoding the binary hologram, the DMD SLM is illuminated with a Gaussian beam which is diffracted into several orders. In order to generate the hologram shown in Figure 2(d), two manipulations are necessary: first, the diffracted light is spatially filtered to recover the first diffraction order. At this point, the filtered electric field should have the exact same profile as the two desired Gaussian beams. Secondly, the filtered light is transformed in order to obtain the Young's interference pattern $I_{in}(x, y)$. In a last step, beam shaping is performed via the optical transformation of the generated hologram, to obtain the two Gaussian beams at the photonic sample plane (2(e)). It has to be noted that it could also be possible to place the sensor directly after the filter; however, it is experimentally quite tricky to manage the positioning of the filter so close to the sensor.

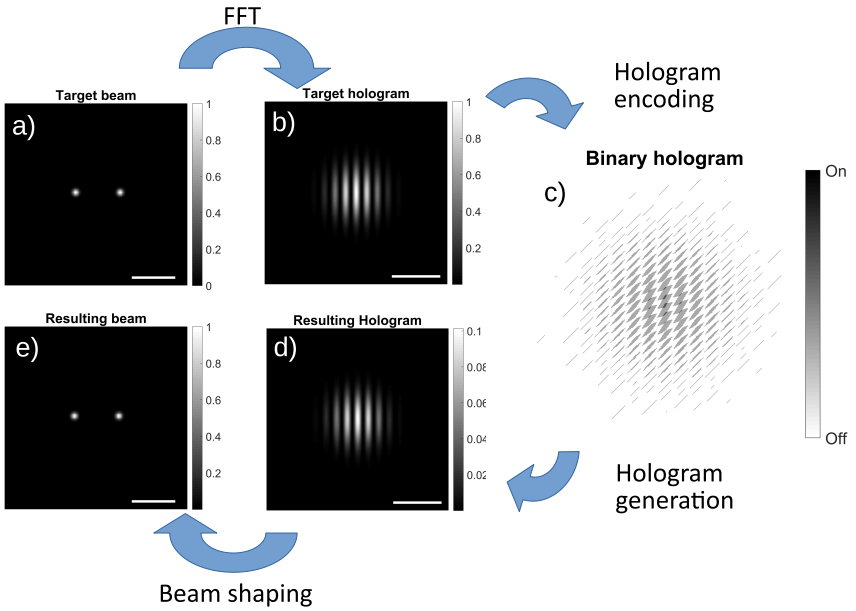

Fig. 2. (a)–(c) Hologram generation process, from the targeted beam shape to the generated binary pattern that will encode the DMD-SLM (numerical steps). (d)–(e) Subsequent optical beam shaping (theses experimental steps are illustrated here by numerical examples).

In order to modulate the signal, N holograms are generated by repeating the above process, where only the phase of one of the two Gaussian beam changes with a $360°/N$ step to produce the phase ramp described by Eq. (2). This way, the generated hologram is the modulated $I_{in}(x, y, t)$, which leads to the phase of one of the two Gaussian beams obtained at the sample level being periodically modulated in time.

Optics EXPRESS

3. Experimental implementation

3.1. Transmission and reflectivity configuration

The hologram generation described above can be experimentally implemented, either in a transmission (Figure 3(a)) or in a reflection (Figure 3(b)) configuration depending on the transparency of the sample substrate and the optical properties of the photonic sensor. For both configurations the set-up can be divided in two blocks: i) the hologram generation block and ii) the beam shaping and Young's interference experiment block. In the hologram generation block the input hologram $I_{in}(x, y, t)$ is produced. In this block a tunable NIR laser fixed at 1300 nm wavelength is expanded to illuminate the DMD SLM. The reflected light from the DMD is transformed into an analog hologram by a 4f system (Lens L_1 and L_2 and spatial filter (SF)). In the beam shaping and Young's interference experiment block, the lens L_3 transforms the input Young's interferometric pattern $I_{in}(x, y, t)$ into the shaped beam (i.e., the two Gaussian beams). The Young's interference experiment is done by the last lens (L_3 in the reflection configuration and L_4 in the transmission configuration). The light passes through a pinhole or a slit (P) centered on the central fringe and is detected by an InGaAs photodiode (PD, model SM05PD4A from Thorlabs). The signal $I_c(t)$ is amplified by a photodiode amplifier (Thorlabs PDA200C) and recorded over time with a NI 9234 acquisition card from National Instruments at 51200 sample/s acquisition rate.

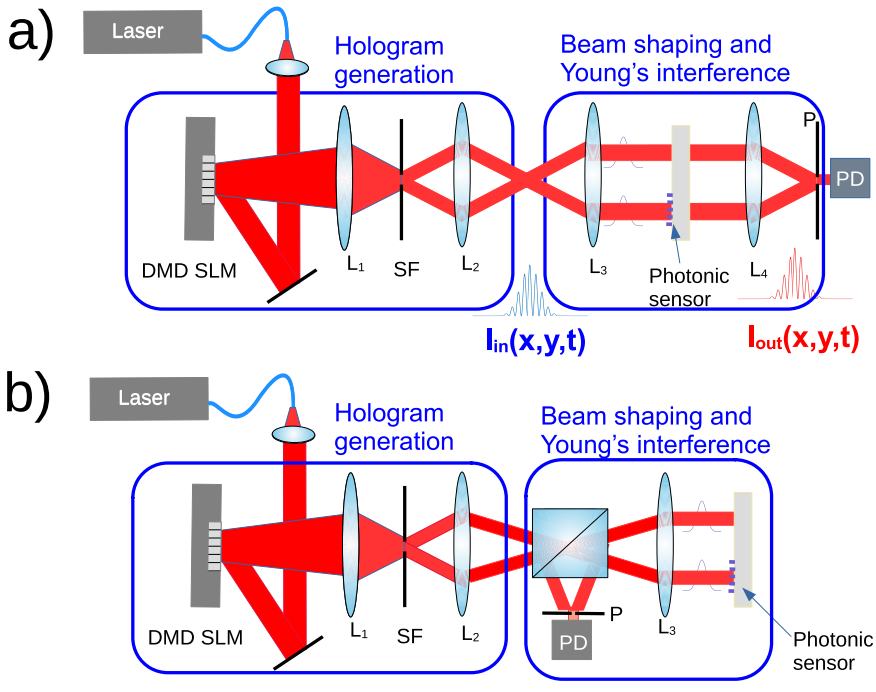

Fig. 3. The experimental set-up: a) in transmission configuration, b) in reflection configuration

3.2. Hologram generation and beam shaping

In Figure 4(a), a generated hologram is shown for a transmission configuration with no sensor (i.e, $s = 1$ and ϕ_{test} is a constant). This hologram, recorded with a SWIR camera, is generated using the center part of a DLP300 DMD from Texas Instruments (340 x 340 pixels while 680 x 340

Optics EXPRESS

available) and two identical lenses L_1 and L_2 with focal length equal to 75 mm. At the Fourier plane of Lens L_3 (focal length 150 mm), the two Gaussian beams are shaped as expected with high fidelity with waist $a = 52\ \mu m$ and spacing distance $D = 520\ \mu m$ (Figure 4(b)). Figures 4(c) and (d) present the cross sections for both the hologram and the two generated beams. As can be seen in Figure 4(d), the experimental shaped beam (blue curve) is very close to the theoretical one (red curve), with the same maximum positions.

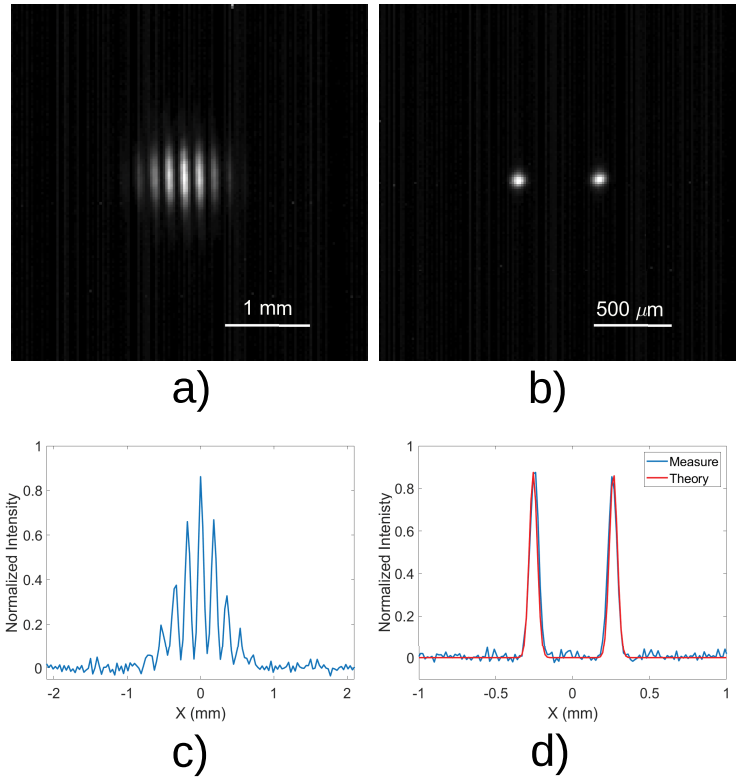

Fig. 4. Hologram sensor in transmission configuration using a DMD with a 680 x 340 micromirrors matrix. a) Experimental hologram showing the Young's interferences pattern generated at the image focal plane of lens L_2. b) Shaped Gaussian beams at the image focal plane of lens L_3. c) and d) show the horizontal intensity cross sections of a) and b) respectively.

3.3. Modulation and demodulation

We have also built the sensor measurement technique in the reflection configuration, using a Vialux V-650L NIR DMD SLM including a 1280 x 800 DLP650LNIR DMD from DLP Texas Instruments. In this case the L_1 and L_2 lenses have a focal length of 75 and 100 mm, respectively, and a NIR Mitutoyo X5 objective lens is used as lens L_3. The frequency modulation of the 100 holograms sequence is $f_{mod} = 80\ Hz$. The $I_n(x, y, t)$ input holograms generate two Gaussian beams with a waist $a = 8\ \mu m$ and separated by $D = 80\ \mu m$. In this set-up, P is a slit with 100 μm width. The tunable laser is fixed at 1300 nm wavelength. The experimental interferometric signal $I_c(t)$ is represented in Figure 5(a). The signal $I_c(t)$ shows a quite pure sinusoidal modulation that follows Eq. (4). It is confirmed by the Fourier analysis of the signal over 100 cycles shown in Figure 5(b): the main peak at 80 Hz is associated to the sinusoidal modulation. Considering

Optics EXPRESS

this Fourier transformation of the interferometric signal $I_c(t)$, we can retrieve both the amplitude $sA_{test}A_{ref}$ and the phase ϕ_{test} from the complex value of the component at $f_{mod} = 80\ Hz$. We can notice in the frequency domain, higher frequency components above f_{mod} are harmonics of the main modulation. These components are generated by the Lee algorithm and not by spurious mechanical effects of the SLM. When we sum all the amplitude of theses harmonics, it represents 11% of the signal whereas the modulation at f_{mod} 89% . This Fourier decomposition shows that the modulated signal is quite pure. But the most important feature in this Fourier spectrum is the ratio between the amplitude at f_{mod} (0.69) and the noise around this frequency (around 2.10^{-5}) which leads to a ratio far better than 5000. This high dynamic range between the component at f_{mod} and the ground floor ensures extracted phase ϕ_{test} with low noise.

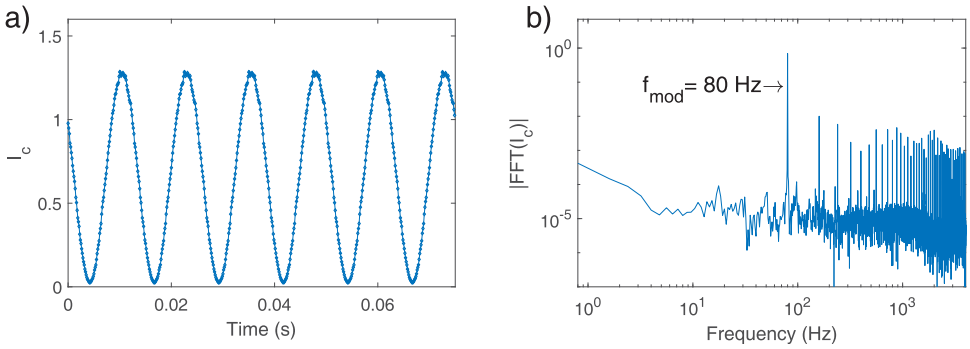

Fig. 5. Modulation and demodulation for hologram sensor in reflection configuration on a mirror surface. In a) the modulated interferometric signal I_c, in b) its Fourier transform.

3.4. *Phase limit measurements and stability*

Before placing a sample with a photonic sensor in the set-up, we have analyzed the stability of the hologram sensors using a mirror on the sample stage of the reflection configuration set-up. As presented in Figure 6, the RMS noise of the phase is 0.039 °, and in general this value lies between 0.03 ° and 0.07 ° over the 30 minutes measurements period. This result shows the good

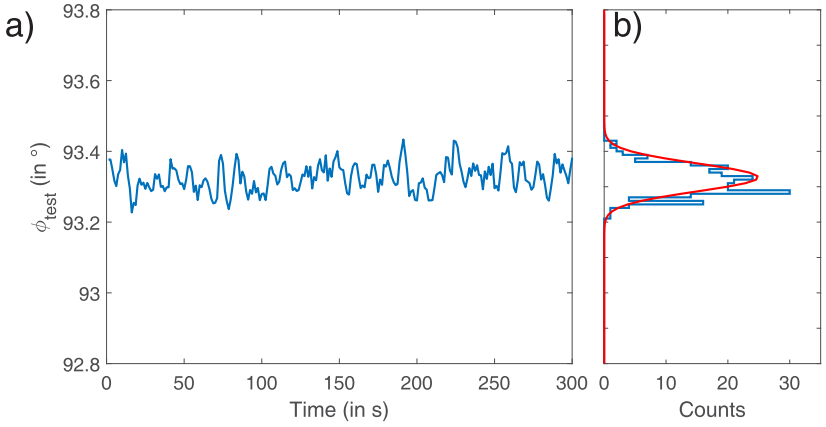

Fig. 6. a) Phase variation over time for a reflection configuration set-up and with a silver mirror as sample and b) corresponding histogram. The red curve in b) is a Gaussian law with a 0.039 ° standard deviation.

Optics EXPRESS

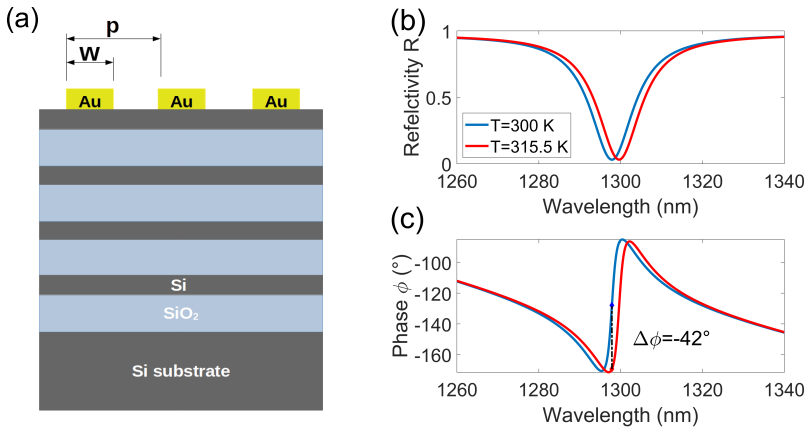

Fig. 7. a) Schematic section of the Tamm Photonic Crystal. Example of theoretical intensity (b) and phase shift (c) of a PC resonance due to temperature variation.

stability of our measurement set-up and experimentally demonstrates RMS noise values that are near the well know limit of 0.01°.

4. Application on a photonic crystal sensor

The interferometric method presented in this work can be validated for sensing applications, using a photonic sensor as a sample. Here, we use a photonic crystal (PC) as the sensing device. The PC is a Tamm plasmon photonic crystal [28]. We study it in this work as a temperature sensor. Tamm plasmon modes are optical states localized at the interface between a dielectric Bragg mirror and a thin metal layer. Figure 7(a) shows an artistic view of the device. The Bragg mirror consists of 4 pairs of Si/SiO_2 layers (thicknesses 107 nm/260 nm) designed to yield high reflectivity in the 1300 *nm* wavelength region. As shown in Figure 8(a), The structured size is a 50 μm x 50 μm square and the top metal structure is a patterned gold layer constituted by a grating of gold stripes with 50 nm thickness, width w = 477 *nm* and periodicity p = 665 *nm*. The optical response of a surface-addressed resonant structure for such PC is characterized by a Fano profile in the reflected spectra; this intensity profile goes along with a phase jump which can be drastic, depending on the interaction between the incident light and the device [20]. The blue curves in Figure 7(b) and (c) show examples of theoretical intensity and phase responses of our Tamm plasmon PC computed by FDTD. Because of the interaction of the transducer with its environment, any change in the device vicinity (temperature variation, adsorption of molecules or biochemical reactions, local refractive index change etc.) leads to a resonance shift, which is illustrated in the red curves of Figure 7(c) in the case of a temperature change. The phase change is reversible when the PC is heated (cooled) the wavelength of the resonance is red (blue) shifted. When performing phase interrogation with the interferometric set-up, the phase shift is measured at a fixed wavelength. The amplitude of the phase variation $\Delta\phi$, which is highlighted by the vertical black line in Figure 7(c), is correlated to the physical quantity (here temperature) to be detected.

The sample is placed in the experimental set-up with the reflection configuration and illuminated at a fixed wavelength that has been chosen to be at the minimum of the peak resonance (i.e, 1297.4 nm in the experimental spectra of Figure 8(c). The sample is heated with a heating stage suited from microscopy (model TC-E35x11 from Bioscience Tools) and supplied with a high stability temperature controller (model TC 1-100-S from Bioscience Tools). The stability and

Optics EXPRESS

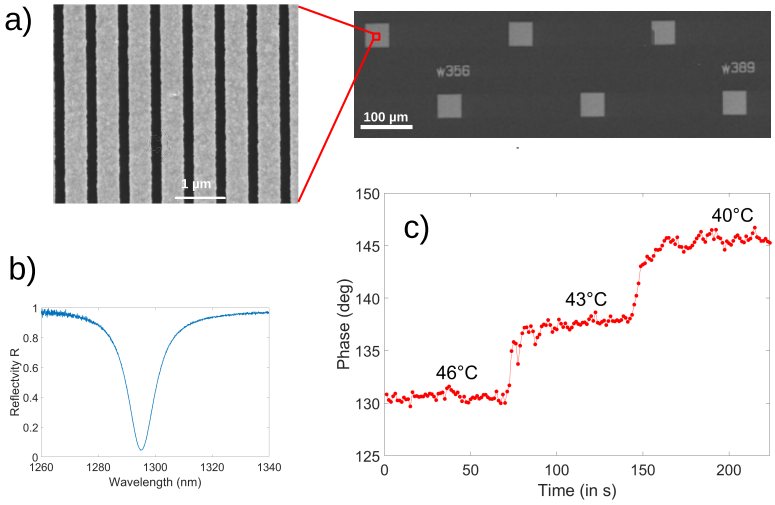

Fig. 8. Phase measurement on a Tamm plasmon photonic crystal during heating. a) Top view SEM image of several photonic crystals and a zoomed view of their nanostructuration. The diamter of the beam size that illuminates the PC at its center is 16 μm which is smaller than the PC size. b) Intensity reflectivity spectra showing the resonance. c) Phase variation over time during cooling of the PC.

precision are around 0.1°C and the temperature values on the sample have been calibrated with a thermographic camera. The phase variation is recorded at the initial fixed wavelength. During the variation of the temperature from 46°C to 40°C by steps of -3°C, the sensor system detects the phase shift with a step of nearly 8° as shown in Figure 8(c). This result demonstrates the ability of the sensor to detect and to follow phase variations of a photonic crystal subjected to temperature variation.

5. Discussion

Our hologram sensing technique presents several advantages that are key in order to reach very low limits of detection. It is very stable and presents very low noise, despite the strong attenuation of light during the propagation from the laser to the detector. This attenuation is due to different contributions: (i) the DMD efficiency is around 1%, which is inherent to SLM diffraction efficiency and to the Lee Method where most of the light is in the other order of diffraction than the first order selected with the spatial filter SF; (ii) the beam splitter and the slit (that filters only a fraction of the central fringe) also induce optical loss. All the losses lead to an attenuation factor of 26 000. Despite this important loss, with a 10 mW laser power and for a transducer yielding a reflectivity $R = 10^{-4}$ at resonance, the noise due to the laser and the detector generate a RMS phase error of 0.01° which is below the experimental phase fluctuations reported above. In others words, regarding phase noise, the optical losses that are intrinsic to our interferometric method are not the limiting factor, and we are able to measure the phase of the transducer, even when the reflectivity intensity is very low.

The slit in front of the photo-detector plays a crucial role in the sensing sensitivity. There is a tradeoff for the choice of the slit width: reducing it induces more losses, but at the same time it improves the fringe visibility and it reduces the angle range of the incident light detected by the photo-detector. Improving the fringe visibility enhances the signal ratio of the extracted amplitude and phase from the measurement. Reducing the angle range is also of high interest in order to measure high phase sensitivities. As discussed in our previous work [29], the phase

Optics EXPRESS

sensitivity of PCs is drastically increased in the case of high-quality factor resonances and/or when reaching the critical coupling, hence leading to higher-performance transducers. But at the same time, this higher phase sensitivity means very sharp jumps of the phase vs. the wavelength. Hence, a wide range of collection angles will smooth the phase jump, and will reduce the phase sensitivity. On our reflection set-up, the angle range $\Delta\theta$ is equal to W_s/f_3 with W_s the width of the slit and f_3 the focal length of lens L_3. This angle range is equal to 0.14° (to be compared with the detection angle using a usual objective lens, which is usually several degrees). This means that our hologram sensing technique enables to measure the phase reflectivity of the photonic device with this small angle aperture, which is well suited for devices yielding very sharp phase jumps.

We do not discuss the LOD of our sensor which depends on both the phase noise of the instrument and the phase sensitivity of the photonic sensor. In an other communication, it will be presented the study of the phase sensitivity versus critical coupling and the physical paramaters of the Tamm plasmon photonic crystal.

Besides its high potential to reach very low limits of detection, our hologram sensing technique offers other technical advantages that can be of high interest for applications. First, it is based on common-path interferometry, which means that an incoherent light source could be used instead of a laser. This property comes from the fact that the interference fringes are included in the Gaussian envelop, and that the difference of the optical path between the two beams is lower than a limit $\Delta\theta$ is equal to W_s/f_3. In our experimental configuration, the ratio D/a is equal to 5, which corresponds to a maximal optical length difference L_c of only 4 μm. This short coherence length traduces very well that the hologram sensor is based on a common path interferometer. As L_c corresponds to the minimal coherence length needed for the optical source, with a value as low as 4 μm a LED or SLED can be used instead of a laser.

Secondly, the versatility of the DMS-SLM leads to large range of functionalities for the presented interferometric method, which go beyond the work presented in this article and open exciting perspectives to expand its field of application. In particular, with the DMD SLM the holograms are reconfigurable, which means that we can simultaneously perform multiplexing and beam shaping:

- i) multiplexing: our beam shape technique by SLM is able to shape many spots instead of two beams (as an array or a matrix of spots) and in the same time we can assign an independent phase modulation for each beam i with a ramp of phase with frequency f_i that follows Eq. (2). By FFT analysis of the photodiode signal each sinusoidal component with its own frequency f_i will be extracted. Consequently, with only one photodiode, we will be able to follow the phase response of each beam that is located on each independent photonic crystal. So we do not need moving stage or scanning sample to process multiplexing.

- ii) beam shaping: with the DMD-SLM the beam shaping possibilities can be pushed further by replacing the Gaussian shape with a beam with a topological charge phase shape. This beam shaping could be used to characterize and/or to optimize the sensing function of photonic sensors with topological charges properties.

And finally, our hologram sensing method is also compatible with further implementations that would increase the amount of information in the detected signal. In the initial set-up with a slit, we have selected the response for an illumination at normal incidence. However, if the slit and the photodetector were removed and replaced by a camera, it would enable to retrieve the reflected or transmitted complex field $\mathbf{s} = s.e^{\phi_{test}}$ for every angle of illumination $\theta_x = x/f_3$ and $\theta_y = y/f_3$ in x and y direction. The angular range of illumination in each direction could be increased by reducing the size a of the Gaussian beam. Using this method, a complex 2D reflectivity diagram can be achieved, leading to a phase sensor with 2D angular interrogation.

Optics EXPRESS

6. Conclusion

In this work, we have proposed an original phase interrogation method for optical sensor applications, which we called hologram sensing. It is a common-path pseudo-heterodyne Young's interferometer. We produce the Young's experiment with two Gaussian spots that are beam-shaped with a digital micro mirror device. The time modulation of the holograms that probe the optical transducer with phase shifting is also allowed by the DMD, which is a fast spatial light modulator. The originality of our interferometric method lies in the generation of an input hologram sequence and in the collection of the perturbed hologram sequence at the output by the optical transducer. We have provided a detailed description of the principle of the phase measurement method, and designed a hologram sensor set-up for optical transducers that works in transmission as well as in reflection. We have shown that the measurement has very good stability with drastic reduction of drift, and that the experimental noise is not limited by the noise of the laser or by the noise of the detection stage. Moreover, we have shown that the noise and resolution of the phase that can be reached are at the state of the art. We have illustrated the possibilities of this method by measuring the phase variation of a resonance on a Tamm plasmon photonic crystal transducer upon heating, and demonstrated that the proposed technique keeps its sensitivity even if the optical resonances yield very low reflected signal. Consequently, it opens up the road for probing sensors at the limit of critical coupling, i.e., devices that provide enhanced sensitivity, hence lower limit of detection. The other originality lies in the shaping and control of the profile of the light.

Funding. European Regional Development Fund (RA 0030195).

Acknowledgment. We acknowledge the European Union and the Rhône Alpes Auvergne Region that granted the INSIDEPACK+ project under reference RA 0030195 beneath the "Fonds Européen de Développement Régional (FEDER)"

Disclosures. The authors declare no conflicts of interest.

Data Availability. Data are available in [30] In this file, the interactive graphic Matlab software that generate the sequence of hologram is provided as well as the data and raw data leading to Figures 5, 6 and 8. Only software that converts raw data to the demodulated signal are not provided. They can be shared at request.

References

1. N. Bellassai, R. D'Agata, V. Jungbluth, *et al.*, "Surface plasmon resonance for biomarker detection: Advances in non-invasive cancer diagnosis," Front. Chem. **7**, 570 (2019).
2. M. Khatib and H. Haick, "Sensors for volatile organic compounds," ACS Nano **16**(5), 7080–7115 (2022).
3. J. Homola, "Surface plasmon resonance sensors for detection of chemical and biological species," Chem. Rev. **108**(2), 462–493 (2008).
4. P. Kozma, F. Kehl, E. Ehrentreich-Förster, *et al.*, "Integrated planar optical waveguide interferometer biosensors: A comparative review," Biosens. Bioelectron. **58**, 287–307 (2014).
5. B. Spackova, P. Wrobel, M. Bockova, *et al.*, "Optical biosensors based on plasmonic nanostructures: A review," Proc. IEEE **104**(12), 2380–2408 (2016).
6. X. Fan, I. M. White, S. I. Shopova, *et al.*, "Sensitive optical biosensors for unlabeled targets: A review," Anal. Chimica Acta **620**(1-2), 8–26 (2008).
7. G. Pitruzzello and T. F. Krauss, "Photonic crystal resonances for sensing and imaging," J. Opt. **20**(7), 073004 (2018).
8. A. V. Kabashin, V. Kochergin, and P. Nikitin, "Surface plasmon resonance bio- and chemical sensors with phase-polarisation contrast," Sens. Actuators, B **54**(1-2), 51–56 (1999).
9. A. V. Kabashin, S. Patskovsky, and A. N. Grigorenko, "Phase and amplitude sensitivities in surface plasmon resonance bio and chemical sensing," Opt. Express **17**(23), 21191 (2009).
10. S. P. Ng, F. C. Loo, S. Y. Wu, *et al.*, "Common-path spectral interferometry with temporal carrier for highly sensitive surface plasmon resonance sensing," Opt. Express **21**(17), 20268 (2013).
11. S. Khan, S. Le Calvé, and D. Newport, "A review of optical interferometry techniques for VOC detection," Sens. Actuators, A **302**, 111782 (2020).
12. A. V. Kabashin, V. E. Kochergin, and A. A. Beloglazov, "Phase-polarisation contrast for surface plasmon resonance biosensors," Biosens. Bioelectron. **13**(12), 1263–1269 (1998).
13. Y.-C. Li, Y.-F. Chang, L.-C. Su, *et al.*, "Differential-phase surface plasmon resonance biosensor," Anal. Chem. **80**(14), 5590–5595 (2008).
14. K. Schmitt, B. Schirmer, C. Hoffmann, *et al.*, "Interferometric biosensor based on planar optical waveguide sensor chips for label-free detection of surface bound bioreactions," Biosens. Bioelectron. **22**(11), 2591–2597 (2007).

Optics EXPRESS

15. V. G. Kravets, F. Schedin, R. Jalil, *et al.*, "Singular phase nano-optics in plasmonic metamaterials for label-free single-molecule detection," Nat. Mater. **12**(4), 304–309 (2013).
16. F. Yesilkoy, R. A. Terborg, J. Pello, *et al.*, "Phase-sensitive plasmonic biosensor using a portable and large field-of-view interferometric microarray imager," Light: Sci. Appl. **7**(2), 17152 (2017).
17. W.-K. Kuo, N.-C. Huang, H.-P. Weng, *et al.*, "Tunable phase detection sensitivity of transmitted-type guided-mode resonance sensor in a heterodyne interferometer," Opt. Express **22**(19), 22968 (2014).
18. P. K. Sahoo, S. Sarkar, and J. Joseph, "High sensitivity guided-mode-resonance optical sensor employing phase detection," Sci. Rep. **7**(1), 7607 (2017).
19. I. Barth, D. Conteduca, C. Reardon, *et al.*, "Common-path interferometric label-free protein sensing with resonant dielectric nanostructures," Light: Sci. Appl. **9**(1), 96 (2020).
20. Y. Tsurimaki, J. K. Tong, V. N. Boriskin, *et al.*, "Topological engineering of interfacial optical tamm states for highly sensitive near-singular-phase optical detection," ACS Photonics **5**(3), 929–938 (2018).
21. T. Čižmár, M. Mazilu, and K. Dholakia, "In situ wavefront correction and its application to micromanipulation," Nat. Photonics **4**(6), 388–394 (2010).
22. G. Lazarev, A. Hermerschmidt, S. Krüger, *et al.*, "LCOS spatial light modulators: Trends and applications," (2012).
23. T. Čižmár and K. Dholakia, "Exploiting multimode waveguides for pure fibre-based imaging," Nat. Commun. **3**(1), 1027 (2012).
24. D. Wang, F.-C. Loo, H. Cong, *et al.*, "Real-time multi-channel SPR sensing based on DMD-enabled angular interrogation," Opt. Express **26**(19), 24627 (2018).
25. M.-X. Chiang, J. Tongpakpanang, and W.-K. Kuo, "Phase measurement of guided-mode resonance device using digital micromirror device gratings," Photonics **8**(5), 136 (2021).
26. W.-H. Lee, "Binary Synthetic Holograms," Appl. Opt. **13**(7), 1677 (1974).
27. S. a. Goorden, J. Bertolotti, and A. P. Mosk, "Superpixel-based spatial amplitude and phase modulation using a digital micromirror device," Opt. Express **22**(15), 17999–8009 (2014).
28. L. Ferrier, H. S. Nguyen, C. Jamois, *et al.*, "Tamm plasmon photonic crystals: From bandgap engineering to defect cavity," APL Photonics **4**(10), 106101 (2019).
29. L. Berguiga, L. Ferrier, C. Jamois, *et al.*, "Ultimate phase sensitivity in surface plasmon resonance sensors by tuning critical coupling with phase change materials," Opt. Express **29**(25), 42162–42175 (2021).
30. L. Berguiga, "Data repository for supplementary materials," MyCoRe (2023), https://mycore.core-cloud.net/index.php/s/tLItby1keeuQthi.